17.2 THE DIURNAL MODE OF SUMMER RAINFALL ACROSS THE CONTERMINOUS UNITED STATES IN 10-KM SIMULATIONS BY THE WRF MODEL

JASON C. KNIEVEL*, DAVID A. AHIJEVYCH, AND KEVIN W. MANNING
National Center for Atmospheric Research, Boulder, Colorado†

1. INTRODUCTION

The diurnal cycle of rainfall is fundamental to many regional climates. It follows that one measure of an NWP (numerical weather prediction) model's skill is the realism of the diurnal cycle in its simulated rainfall. In this paper, we analyze the diurnal cycle of rainfall frequency in simulations by the new Weather Research and Forecasting (WRF) Model and compare the results with the diurnal cycle in observed rainfall inferred from the WSR-88D network.

2. DATA AND METHODS

2.1 Observations

We inferred rainfall from NOWrad™ composites of WSR-88D reflectivity, which are created by Weather Services International (WSI) Corporation. NOWrad™ composites have temporal, spatial, and reflectivity intervals of 15 min, 2×2 km^2, and 5 dBZ. Each pixel's value is the largest reflectivity measured at a time, in a column, above a point. WSI filters bad data in multiple steps, first automatically, then manually.

Instead of converting reflectivities to rainfall rates and averaging them, we chose to analyze the fraction of time (expressed as a frequency) that a reflectivity threshold was met or exceeded at each point. For our large datasets, this produced comparatively smooth fields and reduced effects from any particular rainfall episode. Our approach also minimized the influence of infrequent outliers of extremely high reflectivity, some of which were artifacts that escaped quality control at WSI. The Z-R relationship we chose to convert reflectivity factor, Z, to rainfall rate, R, is

$$Z = 300R^{1.4}, \tag{1}$$

the standard relationship for reflectivity from WSR-88Ds (Fulton et al. 1998). According to this equation, 15 dBZ = 0.2 mm h^{-1}, which was our threshold for calculations of rainfall frequency.

* *Address correspondence to:* Dr. Jason Knievel, NCAR, P.O. Box 3000, Boulder, CO 80307-3000; knievel@ucar.edu.

† The National Center for Atmospheric Research is sponsored by the National Science Foundation.

2.2 Numerical simulations

The numerical simulations are from preliminary, or *beta*, versions of the WRF Model, and are for the conterminous United States during June–August 2003 at grid intervals of 10 km. These simulations are a subset of those that have been run experimentally in real time at NCAR, twice per day, at various grid spacings, since 2001. Because one purpose of the real-time runs at NCAR is to evaluate and improve the model, the code has not been static since 2001. However, the code for the 10-km simulations was static from June to August 2003, which is why we selected these three months.

Boundary and initial conditions were on 40-km grids from the Eta Model run at the National Centers for Environmental Prediction (NCEP). There were 35 vertical levels in the WRF simulations. Cumulus parameterization was by the Kain-Fritsch scheme after modification for implementation in the Eta Model. Microphysical parameterization was by the 2-category scheme developed by Ferrier. The planetary boundary layer was parameterized by the MRF scheme. The land surface model comprised a thermal diffusion scheme with 5 layers of soil. The shortwave radiation scheme was based on code developed by Dudhia (1989), the longwave on code developed by Mlawer et al. (1999). Output was hourly. We confined our analyses to simulations initialized at 0000 UTC. In order to minimize effects of the initialization, we analyzed each 24-h forecast interval starting at the ninth hour.

2.3 Fourier analyses

We quantified the diurnal cycle of rainfall frequency through Fourier decomposition. Frequencies from NOWrad™ data were averaged over sets of four consecutive times (0545, 0600, 0615, and 0630 UTC, for example) and assigned to a single time within that set (0600 UTC, for example) in order to convert 15-min data to hourly data. Hourly output from the WRF Model (1-h accumulated rainfall ending at 0600 UTC, for example) was assigned to a time at the midpoint of the output interval (0530 UTC, for example). Sine curves of varying period were then fitted to the 24 hourly values in each dataset using a least-squared-error method. Herein we feature only the zeroth and first harmonics. The zeroth

harmonic corresponds to the mean rainfall frequency for the entire three months of study. The first harmonic corresponds to the diurnal cycle of rainfall frequency. For the first harmonic, we calculated the maximum's amplitude and its timing, or phase. Because amplitude is a function of the mean frequency (0th harmonic), we normalized the amplitude by dividing it by the mean, a technique used by Wallace (1975), among others. The normalized amplitude represents the strength of the diurnal cycle. Our reference for the timing of the cycle's maximum was local solar time, as calculated from the phase of the first harmonic and longitude at each grid point.

2.4 Caveats

The simulations and observations should be compared cautiously. First, the two datasets have different temporal and spatial resolutions. In particular, in the NOWrad™ data each hourly occurrence of rainfall is a multiple of 0.25 because each hourly value is an average of four 15-min values. In the simulations, however, each hourly value is simply a multiple of 1.0; either the threshold was met (1.0), or it was not (0.0).

Second, although the WSR-88D network detects rainfall over more of the nation, and at better resolutions, than any previous networks did, there are gaps in the network's coverage. Gaps are worst in the West, where mountains block radar beams. In addition, a radar's detection efficiency depends on range. Some artifacts of this dependency escaped WSI's quality control and appear in the figures below (e.g., the circular patterns in the central U. S. apparent in Figs. 1 and 3). In numerical simulations there are no counterparts to beam blocking and detection efficiency.

Third, the Z-R relationship is problematic. No single relationship applies equally well for all radars, at all times, in every location (Doviak and Zrnic 1993; Crosson et al. 1996). Moreover, Z-R relationships are not intended for composites of columnar maximum reflectivity, such as NOWrad™ , in which the vertical distribution of reflectivity is lost. When Crosson et al. (1996) applied Z-R relationships to composites of reflectivity from WSR-57s, they found that rainfall rates diagnosed for Florida thunderstorms were too high by roughly a factor of two. Fortunately, in the case of our research, problems with equating reflectivity to rainfall rate were partially mitigated by our choice of rainfall frequency instead of rainfall, itself, as the foundation of our analyses.

3. RESULTS

3.1 Mean frequency

Rainfall was more frequent in the simulations than in the observations (cf. Figs. 1 and 2). The discrepancy was especially large over the Atlantic Ocean, the Gulf of Mexico, and parts of Canada, where differences were a factor of two in some places, four in others. According to our tests of frequencies at higher thresholds, light rain accounted for most of the overprediction. We have not yet tried to isolate the problem but suspect that the model's cumulus parameterization may be generating light rain too often or for too long in environments that are only weakly unstable. Because no single color table is simultaneously appropriate for the different ranges of frequencies in both datasets, we include a second plot with different shading for the observations (Fig. 3).

Overall differences in magnitude aside, the locations of many extreme frequencies in the simulations were similar to those in the observations (cf. Figs. 2 and 3).

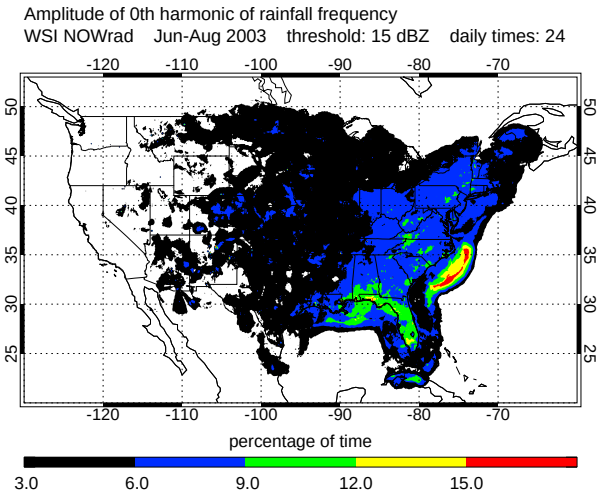

Figure 1: Mean rainfall frequency diagnosed from NOWrad™ composites for Jun–Aug 2003.

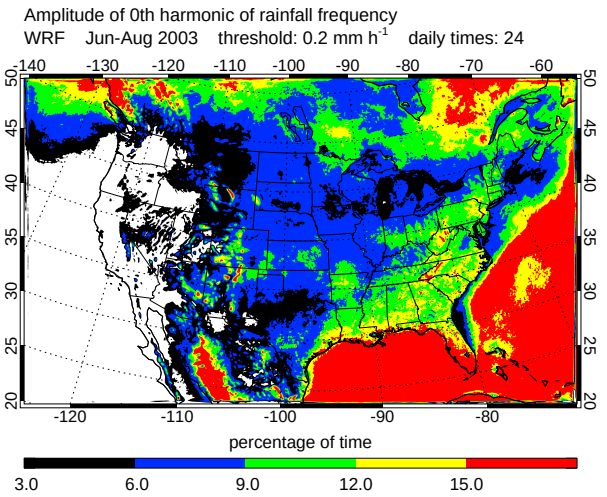

Figure 2: Mean rainfall frequency in simulations by the 10-km WRF Model for Jun–Aug 2003.

In both datasets, an expansive arc of frequent rainfall extended from the northern Texas coast, through the Southeast and parts of the Appalachians, and ended in the Ohio Valley, Mid-Atlantic, and parts of New England. In particular, frequent rainfalls over the Gulf Stream off the Carolina coasts and over Florida stand out. The latter was probably due to afternoon thunderstorms forced by horizontal convergence and lifting at the leading edge of the sea breeze (e.g., Byers and Rodebush 1948; Frank et al. 1967).

The observations and simulations also share many maxima in rainfall frequency that are more localized. Some of these, for example, were in Arkansas, New Mexico, and Colorado. All these locations are mountainous. Sunshine on mountains induces circulations wherein lower-tropospheric air converges and rises, often generating daily thunderstorms during the summer (e.g. Reiter and Tang 1984). The highly localized maxima appear to have been more directly collocated with mountains in the simulations than in the observations. For instance, in Wyoming, Colorado, and New Mexico, frequencies $\geq$15% coincided almost exactly with the highest terrain (Fig. 2). This subtle difference between the simulations and the observations may be a sign that the WRF Model exaggerated lower-tropospheric convergence in response to solar heating. It may also be a sign that the WSR-88D network did not fully observe rainfall over the highest peaks in the Rockies. The latter is certainly responsible for part of the two datasets' apparent differences in rainfall frequency in the West (cf. Figs. 2 and 3). Indeed, gaps in the WSR-88D coverage exaggerated the infrequency of rain in the entire western third of the nation, which makes impossible any detailed comparisons of simulations and observations over that region as a whole (more limited studies are certainly still possible).

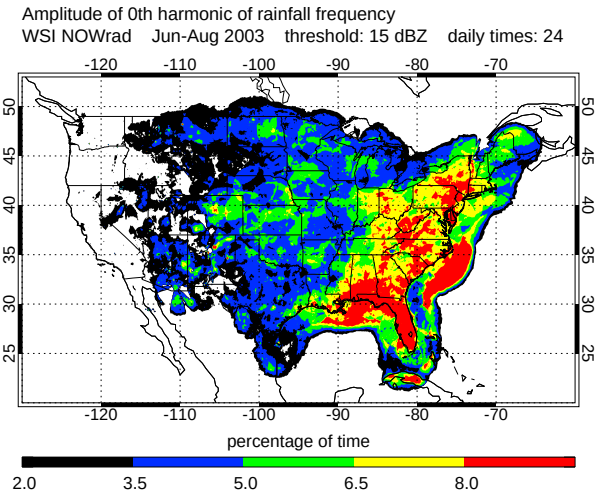

Figure 3: Same as Figure 1 except for shading.

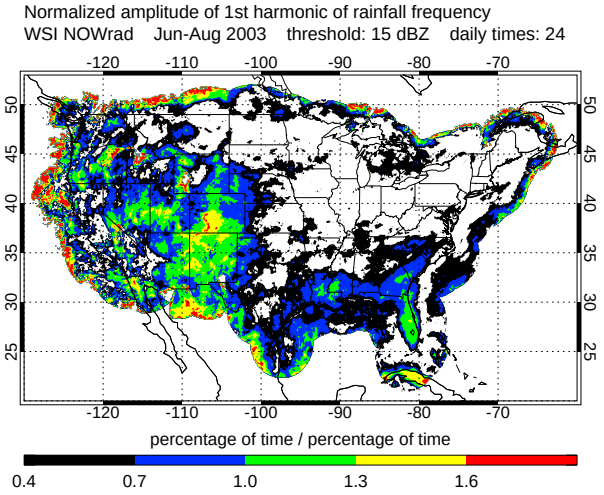

Figure 4: Strength of the diurnal cycle of rainfall frequency diagnosed from NOWrad^{TM} composites for Jun–Aug 2003.

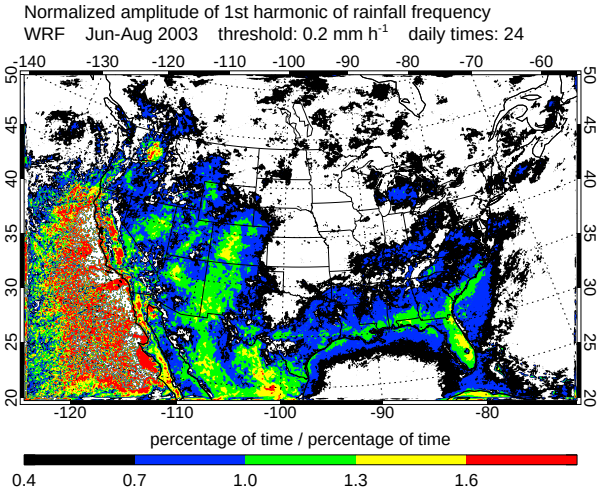

Figure 5: Strength of the diurnal cycle of rainfall frequency in simulations by the 10-km WRF Model for Jun–Aug 2003.

3.2 Strength of the diurnal cycle

The strength and gross spatial distribution of the WRF Model's diurnal cycle of rainfall frequency were similar to those in the observations (cf. Figs. 4 and 5). In both datasets, the strongest diurnal cycles were in the Southeast, near the Gulf Coast, in the lower Mississippi Valley, in the western High Plains, and in mesoscale patches throughout the intermountain West. Both datasets also exhibited a moderate diurnal cycle in rainfall frequency in eastern Michigan and southeastern Ontario.

The diurnal cycle of rainfall frequency in the WRF Model was stronger in the Ohio Valley than was observed. There were also a number of smaller regions in which the model's diurnal cycle apparently was unrealistically strong, such as in the lee of the Cascades in

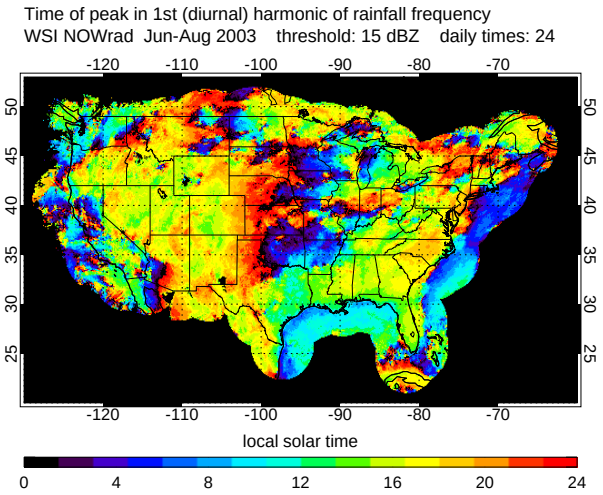

Figure 6: Timing of the peak in the diurnal cycle of rainfall frequency diagnosed from NOWrad^{TM} composites for Jun–Aug 2003.

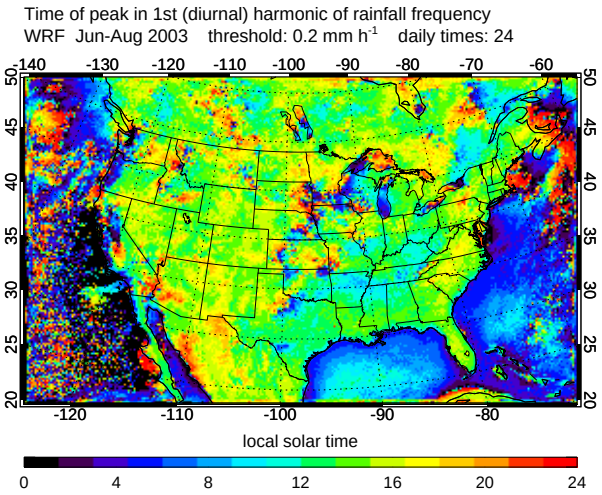

Figure 7: Timing of the peak in the diurnal cycle of rainfall frequency in simulations by the 10-km WRF Model for Jun–Aug 2003.

eastern Washington, in California's Sacramento and San Joaquin Valleys, and over the Pacific Ocean off the California Coast (Fig.5). However, simulated rainfall was so infrequent in these regions (Fig. 2) that the normalized amplitude of the 1st harmonic is probably not physically meaningful. The extreme noise in the 1st harmonic over the eastern Pacific Ocean further supports this supposition (Fig. 5). Gaps in radar coverage caused similar problems in the observations, such as in central Idaho and southwestern Wyoming (Figs. 3 and 4).

The simulations were generally consistent with the observations in many of the broad regions of the nation where the diurnal cycle of rainfall frequency was weak: most states bordering Canada, the central Mississippi Valley, the eastern Great Plains, the Mid-Atlantic, and New England (cf. Figs. 4 and 5).

3.3 Timing of the maximum in the diurnal cycle

For much of the nation, the phases in the observed and simulated diurnal cycles were roughly similar (cf. Figs. 6 and 7). In both datasets, diurnal rainfalls were most frequent in the afternoon and early evening in many regions, especially in the states bordering the Atlantic Ocean and in the western third of the nation. In the observations, early-afternoon diurnal rainfall at high elevations in the West was followed by late-afternoon and early-evening rainfall at low elevations (Fig. 6). The same link between elevation and timing of diurnal rainfall also appeared in the simulations, although a bit less distinctly (Fig. 7).

Although the two datasets' diurnal cycles were roughly in phase, the model produced slightly earlier peaks in frequency over large regions of the nation (cf. Figs. 6 and 7). The difference was especially marked in the Appalachians, in the southern Mississippi Valley, and in much of the intermountain West. Also, in a narrow strip along the Atlantic Coast from Myrtle Beach, South Carolina to the southern tip of the Florida Peninsula, the model's peak in diurnal frequency was a few hours earlier than the observed mid-afternoon peak, which suggests that sea breezes in the WRF Model may have been poorly timed, or that the cumulus parameterization may have performed unrealistically.

The single most striking discrepancy in the timing of the diurnal cycle between the simulations and the observations, however, was in the central part of the nation. There, consistent with climatographies by many others (e.g. Kincer 1916; Balling 1985), the observed peak in diurnal rainfall was nocturnal (the division between red and black shading in Fig. 6 marks local midnight). The peak shifted systematically from late evening in the High Plains, to the hours just before sunrise in the Missouri and upper Mississippi Valleys. The WRF Model greatly underpredicted the strength and areal extent of this nocturnal peak. Only in a few, isolated parts of the central United States, such as in eastern Montana, eastern South Dakota, southern Minnesota, and western Kansas, for example, were there localized nocturnal peaks in the simulations (Fig. 7). Morning and afternoon peaks were far more common. It is not that the WRF Model produced too little rain or too infrequent rain over the Great Plains—on the contrary, simulated rainfall was quite frequent there (Fig. 2). Instead, the model failed to capture the nocturnal dominance of rainfall in the Great Plains, perhaps partly because of unrealistically frequent rainfall at other times of the day.

We suspect this discrepancy in timing was due mostly to the unrealistic treatment of the organization and

motion of the nocturnal mesoscale convective systems (MCSs) that account for so much of the Plains' summer rainfall (Maddox 1980; Fritsch et al. 1981). There is evidence that convective systems whose cumulus convection is parameterized—as it was in the 10-km WRF Model—tend to travel mostly by advection because the propagative component in their motion is all but lost (Davis et al. 2003). If our suspicion is correct, then simulations at grid spacings that explicitly resolve convective rainfall should produce more realistically timed peaks in diurnal rainfall frequency in regions where convective systems rely on their cold pools for propagation. We are currently exploring this topic, was well as other topics brought to light in the datasets we analyzed.

Acknowledgments. We benefited from informative and lively discussions with G. Bryan, C. Davis, and J. Dudhia, and from the assistance of J. J. Gourley, G. Stumpf, and W. Wang. The Global Hydrology Resource Center (GHRC) of the Marshall Space Flight Center supplied the NOWrad™ data from WSI, Inc. This is an expansion of work started by Davis et al. (2003).

REFERENCES

Balling, R. C., Jr., 1985: Warm season nocturnal precipitation in the Great Plains of the United States. *J. Climate Appl. Meteor.*, **24**, 1383–1387.

Byers, H. R., and H. R. Rodebush, 1948: Causes of thunderstorms of the Florida Peninsula. *J. Meteor.*, **5**, 275–280.

Crosson, W. L., C. E. Duchon, R. Raghavan, and S. J. Goodman, 1996: Assessment of rainfall estimates using a standard Z-R relationship and the probability matching method applied to composite radar data in central Florida. *J. Appl. Meteor.*, **35**, 1203–1219.

Davis, C. A., K. W. Manning, R. E. Carbone, S. B. Trier, and J. D. Tuttle, 2003: Coherence of warm-season continental rainfall in numerical weather prediction models. *Mon. Wea. Rev.*, in press.

Doviak, R. J., and D. S. Zrnic, 1993: *Doppler Radar and Weather Observations*. Academic Press, 562 pp.

Dudhia, J., 1989: Numerical study of convection observed during the Winter Monsoon Experiment using a mesoscale two-dimensional model. *J. Atmos. Sci.*, **46**, 3077–3107.

Frank, N. L., P. L. Moore, and G. E. Fisher, 1967: Summer shower distribution over the Florida peninsula as deduced from digitized radar data. *J. Appl. Meteor.*, **6**, 309–316.

Fritsch, J. M., R. A. Maddox, and A. G. Barnston, 1981: The character of mesoscale convective complex precipitation and its contribution to warm season rainfall in the United States. Preprints, *4th Conference on Hydrometeorology*, Reno, NV, Amer. Meteor. Soc., 94–99.

Fulton, R. A., J. P. Breidenbach, D.-J. Seo, and D. A. Miller, 1998: The WSR-88D rainfall algorithm. *Wea. Forecasting*, **13**, 377–395.

Kincer, J. B., 1916: Daytime and nighttime precipitation and their economic significance. *Mon. Wea. Rev.*, **44**, 628–633.

Maddox, R. A., 1980: An objective technique for separating macroscale and mesoscale features in meteorological data. *Mon. Wea. Rev.*, **108**, 1108–1121.

Mlawer, E. J., S. J. Taubman, P. D. Brown, M. J. Iacono, and S. A. Clough, 1999: Radiative transfer for inhomogeneous atmosphere: RRTM, a validated correlated-k model for the longwave. *J. Geophys. Res.*, **102**, 16663–16682.

Reiter, E. R., and M. Tang, 1984: Plateau effects on diurnal circulation patterns. *Mon. Wea. Rev.*, **112**, 638–651.

Wallace, J. M., 1975: Diurnal variations in precipitation and thunderstorm frequency over the conterminous United States. *Mon. Wea. Rev.*, **103**, 406–419.